Investigating Protein Unfolding and Stability Using Chaotropic Agents and Molecular Dynamics Simulation

Rohit Shukla and Timir Tripathi

Abstract Protein folding and unfolding processes follow a thermodynamically favourable transitional path. The folding process occurs on a timescale in the order of milliseconds; therefore, observing the correct transitional pathway is challenging. However, with the advancement of computer science, it is now possible to decipher the structural level changes in the folding pathway of the protein using the molecular dynamics (MD) simulation. The MD simulation can provide detailed information about various energetic terms, structural parameters, etc. One can calculate the secondary structure changes with respect to time using MD simulation and correlate them with the CD spectra results. It can also generate thousands of snapshots that can be used to determine accurate unfolding pathways through structure visualization. In this chapter, we describe how chaotropic agents and MD simulation can be used in combination to study the stability and unfolding process of a protein. We also discuss the software used in the MD simulation with a detailed methodology of the GROMACS tool. Lastly, we take two case studies to show the process of urea and GdnHCl-induced denaturation of proteins analysed through MD simulation.

Keywords Urea · Guanidine hydrochloride · Unfolding · Stability · Dynamics · Folding · Denaturation

R. Shukla
Molecular and Structural Biophysics Laboratory, Department of Biochemistry, North-Eastern Hill University, Shillong, India

T. Tripathi (✉)
Molecular and Structural Biophysics Laboratory, Department of Biochemistry, North-Eastern Hill University, Shillong, India

Regional Director's Office, Indira Gandhi National Open University, Regional Centre Kohima, Kohima, India

P. Saudagar, T. Tripathi (eds.), *Protein Folding Dynamics and Stability*,
https://doi.org/10.1007/978-981-99-2079-2_10

1 Introduction

The protein unfolding studies often involves the use of chaotropic agents such as urea and guanidinium hydrochloride (GdnHCl), which reduce the stability of the native protein by destabilizing the hydrophobic interactions between various amino acids [1]. They are widely used for protein unfolding analysis, but the exact mechanism of action is still a mystery. It is well established that protein stability depends on the hydrogen bonding network of the protein with the solvent and intramolecular hydrogen bond interactions [2]. A proper hydrogen bond network is required for a protein to function correctly. Several studies have shown that chaotropic agents can directly bind to the protein or bind with the solvent and alter the properties of the solvent [3–9]. In other cases, the presence of chaotropic molecules also breaks the hydrogen bond network between water molecules, which induces the weakening of the hydrophobic effects. The effect of hydrogen bond disruption due to chaotropic agents is similar to the temperature and pressure-induced hydrogen bond network disruption for the denaturation of the protein [10, 11]. Additionally, the direct binding of the chaotropic molecules with the proteins may weaken the hydrophobic interactions between the non-polar amino acids responsible for stabilizing native proteins.

The folding energy difference between the well-folded and unfolded proteins is typically between 5 and 10 kcal/mol. The unfolded protein is 5–10 kcal/mol less stable than the corresponding native protein. During folding, multiple forces weaken simultaneously with several conformations between native to unfolding transitional states [12], indicating the level of complexity in understanding the protein unfolding and folding process. It also suggests that multiple factors are involved in unfolding/folding processes that should be carefully examined [13, 14]. There are a lot of limitations in experimental methods for studying the protein folding mechanism. They cannot provide detailed visual information about the transitional intermediates during protein unfolding from the nanosecond to the microsecond time scale [15]. They are also expensive in terms of money and labour. The currently available computational approaches can simulate the protein at a microsecond time scale in the presence of denaturants or temperature and can determine the exact unfolding steps in the form of complete trajectories saved at different snapshots. During simulation, several energy parameters can be analysed as well as the detailed insight molecular mechanism of unfolding can be investigated. These trajectories can be analysed using several software, and a lot of meaningful information can be extracted. With the support of graphical processing units (GPUs), currently, supercomputers can perform microsecond time simulation within a day and store petabytes of data. The simulation of a single virus is also possible [16]. However, the addition of solvent and other molecules in the simulation can increase the computational cost and complexity of the simulation result analysis [17–19].

2 Basic Concept of Protein Folding

Anfinsen's hypothesis shifted the concept of protein folding from the disulphide bridge protein folding theory towards the complete protein folding analysis through the eyes of computer scientists or polymer physicists in 1973 [20]. One had to cease thinking in terms of atomic coordinates to demonstrate the uniqueness (stability) of the native structure. It was stated that the necessary pieces of knowledge for folding must be present in the sequence, which was established as the Anfinsen thermodynamic hypothesis [21]. It essentially assumes that the sequence controls the interactions present in the native structure. This is the central idea behind the fascinating intersection of two major lines of research into the prediction of protein structure and the study of protein folding kinetics [22, 23]. Protein folding occurs through an enormous number of possible conformations that cannot be calculated through conventional chemical methods. Levinthal's paradox describes the astronomical number of local minima in the conformational space and the resulting inability to completely explore all conformational spaces. It has been established that even a straightforward explanation of protein folding based on the hydrophobic/hydrophilic model on a cubic lattice is nondeterministic polynomial (NP)-complete in this regard [24]. Overall, the link between sequence and structure and the elucidation of folding processes are challenging issues that are listed among the most significant scientific questions of the twenty-first century [25]. By virtue of their fundamental characteristics, Levinthal's paradox and Anfinsen's hypothesis appear at odds. To assure convergence towards the native state within a definite time, the folding process must first be constrained along a particular path (kinetic control). Conversely, the interim path (thermodynamic control) is comparatively irrelevant because it relies on the function, which is biased towards the final confirmation of the protein. Within the framework of the landscape theory of protein folding, in which both types of regulation are acknowledged, these contradictory criteria become consistent [26, 27]. According to the present theory, parallelization makes more sense early in the folding process and becomes more sequential in the latter stages [28, 29].

3 Chaotropic Agents and Their Mechanism of Action

The chaotropic agents (chaotropes) are chemical entities that disrupt the structure of biological macromolecules, such as nucleic acids and proteins, via the denaturation process. These molecules disrupt the non-covalent interactions such as van der Waals forces, hydrogen bonds, electrostatic interactions, and hydrophobic effects and increase the entropy of the system. The tertiary structure of well-folded biomolecules depends on these non-covalent forces; hence, increasing the concentration of chaotropes in the solution leads to the destabilization of protein followed by denaturation and reduced enzyme activity. The proper folding of a protein is depended on the hydrophobic interactions between the amino acids. Due to the

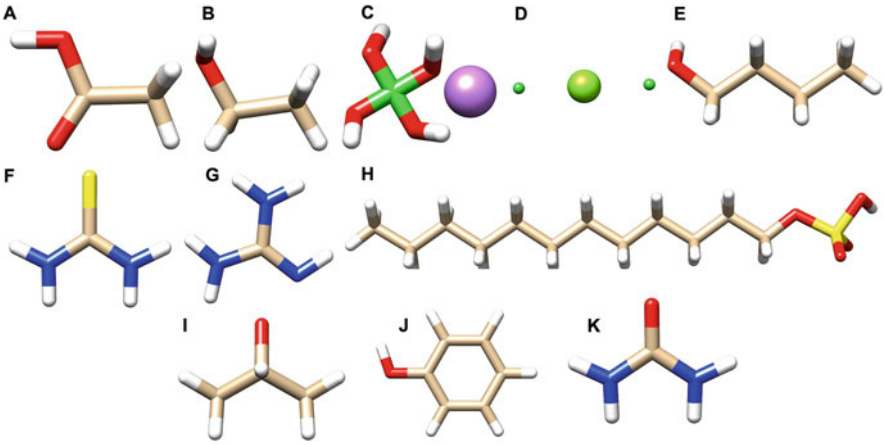

Fig. 1 Chemical structures of a few chaotropic agents. (**a**) lithium acetate, (**b**) ethanol, (**c**) lithium perchlorate, (**d**) magnesium chloride, (**e**) n-butanol, (**f**) thiourea, (**g**) guanidinium chloride, (**h**) sodium dodecyl sulphate, (**i**) 2-propanol, (**j**) phenol and (**k**) Urea

disordered water molecules, the chaotropic solutes reduce the net hydrophobic effects of the hydrophobic regions. This leads to the solubilization of the protein's hydrophobic regions via denaturation. This is also implicated in the case of hydrophobic regions of the lipid bilayers, where a high chaotropic concentration leads to cell lysis by disrupting membrane integrity [30].

The dissociation of chaotropes in solution results in different chaotropic effects. While the chaotropic solvents such as ethanol affect the non-covalent intramolecular forces, the chaotropic salts affect the charged interactions such as salt bridge, etc. A strong hydrogen bond network in proteins is observed in the non-polar medium; therefore, chaotropic salts that can increase the chemical polarity can affect the hydrogen bond network. This happens due to the smaller number of water molecules that can effectively solvate the ions. It leads to the ion–dipole interactions between the hydrogen bonding species and salts which are stronger and more favourable than normal hydrogen bonding [31, 32]. The common chaotropic agents are urea, guanidinium chloride (GdnHCl), thiourea, and sodium dodecyl sulphate (SDS). The chemical structure of a few chaotropic agents is shown in Fig. 1.

4 Molecular Dynamics (MD) Simulation

The molecular dynamics (MD) simulation method was introduced in the 1970s [33, 34]. Currently, with the improvement of computational power, it can be used to simulate from thousands of atoms to the complete virus, proteins, nucleic acids, nucleosomes [35, 36] or ribosomes [37, 38], etc., using the explicit water models. Today, simulations of ~50,000–100,000 atom size systems are in routine practice, and even simulations of more than 1,000,000 atoms are also possible when good computational facilities are available. This was made possible due to the improvement in the MD algorithms and new computing capabilities from the past few decades.

The input structure of any biomacromolecule can be obtained using computational modelling tools or experimental methods [39]. The simulated systems can be represented at different levels of time scale. The atomistic representation model is the best for the reproduction of actual systems. Although, in the case of long simulations or large biological systems, the coarse-grained representation is leading popularity [40]. There are many representation approaches, but the explicit solvent model is the simplest, most popular, and most effective [41–46]. However, increasing the system size in this model increases the size of simulated systems. This solvent model can achieve the solvation effects that happen in a real solvent, including those of entropic origin, like the hydrophobic effect. After building the complete system, using the deriving equations, the forces that act on each atom can be obtained using the force field. In the force field, the potential energy is inferred from the molecular structure [47–52]. The complex equations represent the force field terms which are easy to calculate. There are several simple molecular features that characterize the force field terms, such as bond angles and length, which are represented by springs, bonds rotations, and Lennard-Jones potential represented by periodic functions, electrostatic and van der Walls interaction calculation by Coulomb's law. These terms guarantee that force and energy calculations be very fast for large biological systems. Currently, the parameterization of the force field differs in various atomistic molecular simulations. There are several parameters in the force field which cannot be interchanged, and also, not all force fields allow to represent the all-molecule types though the simulation trajectories and analysis for all the force fields are similar [53, 54]. When the acting forces on each atom are calculated, Newton's classical law of motion is utilized for the acceleration and velocities calculation, including the update of the position of each atom. The MD system movement integration is done using numerical methods; therefore, to avoid instability, a time step shorter than the fastest movement in the molecules is used. This short-time integrator usually lies between 1 and 2 fs for the atomistic simulation and plays a crucial role in the overall simulation.

The long microsecond simulations hardly scratch the time scales for the biological systems and require iterating over the calculation cycle 10^9 times. The coarse-grained simulations are generally better with these limitations. They use a more simplified MD system and represent larger time steps for integration; hence, they can

run the large-scale simulation of large biomacromolecules with good accuracy. The long simulations can run with several advantages that include fine-tuning several energetic parameters and parallelization of the simulation by using graphical processing units (GPUs) that can increase accuracy and improve the simulation speed. The current generation of computers can parallelize the process, which leads to faster MD simulation.

Several MD simulation software are available, and the most widely used are CHARMM [55], GROMACS [56], AMBER [57] and NAMD [58]. These software are well compatible with the messaging passing interface (MPI). Due to a large number of cores in the computers, the MPI can significantly increase the computation power and reduce the computational time. The MD simulation process can be divided into multiple CPU cores that can reduce computational time; this technique is known as spatial decomposition. The part of the complete system is used for the simulation in each processor. This division of MD simulation systems is based on the particle's position in space and not on the list of particles. The region of the space is dealt by each processor instead of the particles present in the MD simulation system. The processor communication is also reduced because only the neighbouring regions of the simulation share information among them [59]. Nowadays, GPUs are becoming the breakthrough in the case of MD simulation due to their ability to accelerate the simulation speed. The currently available MD simulation tools are compatible with GPUs, and even some MD simulation programs, such as ACEMD [60], are written to run on GPU systems. The combination of CPUs and GPUs is the default strategy in the case of atomistic simulations. Currently, high-performance computing (HPC) is the most popular among computational scientists, while GPU development is leading to the greater use of personal computers for atomistic simulations than HPC.

5 Application of MD Simulation in Investigating Protein Unfolding

As described earlier, MD simulation can mimic the in vivo conditions and can provide information on the real dynamics of the system, including effects of mutation in a protein [61–63], protein–ligand interactions [64–67] and protein unfolding [68–70]. The stepwise methodology of the MD simulation process is briefly described below [71, 72].

1. The biological macromolecules should be prepared. The structure may be modelled if an experimental structure is unavailable in the PDB (https://www.rcsb.org). All the hydrogen atoms should be added to the PDB structure.
2. The PDB file should be placed in a box, which can be cubic, dodecahedron, etc.
3. The explicit water molecules should be filled into the box.
4. The concentration of chaotropes should be calculated in the number and added to the simulation box by replacing the water molecules.

5. The MD systems should be neutralized by adding ions.
6. Energy minimization should be performed to remove the steric clashes of the systems caused by the addition of water and chaotropic agents.
7. The number of volumes and temperature (NVT) and the number of pressure and temperature (NPT) simulations should be run to fix the volume, pressure and temperature of the system. After this simulation, the quality of the system can be assessed by plotting all the graphs (pressure, volume, temperature, etc.).
8. Finally, the MD simulation should be run, and values should be saved at 1 to 2 fs time intervals.
9. Lastly, the obtained trajectories should be pre-processed by removing the periodic boundary condition (PBC) artifacts. Several results can be obtained in the form of various graphs, such as root mean square deviation (RMSD), root mean square fluctuation (RMSF), radius of gyration (Rg), solvent accessible surface area (SASA), principal component analysis (PCA), and secondary structure analysis.
10. The trajectories can also be visualized, and the unfolding of the biomacromolecules can be recorded in the form of a trajectory. These graphical and visual analyses can give a glimpse of the complete unfolding process of proteins.

These steps are generally used in all the MD simulation protocols to perform the unfolding analysis of a protein. The graphical user interface (GUI) simulation software such as Desmond and YASARA can be used for this process in a few steps, while the command lines tools such as AMBER and GROMACS complete it in many steps. The general methodology and concept are the same for all the software. Now we discuss two case studies of protein unfolding using urea and GdnHCl.

6 Case Studies

6.1 Urea-Induced Unfolding

We have reported the urea-induced unfolding of the *Acinetobacter baumannii* UDP-N-acetylglucosamine enolpyruvyl transferase (AbMurA) [69]. The structural and unfolding features of AbMurA were analysed using multiple spectroscopic methods, including circular dichroism and fluorescence spectroscopy [73]. The data showed the protein unfolds in a three-state manner with the presence of an unfolding intermediate at 3.5 M urea. The spectroscopic data was complemented using data from multiple 100 ns MD simulations [69]. To study the unfolding behaviour of the AbMurA enzyme, we created six systems where we placed the AbMurA in water, 3.5 M, and 8.0 M urea, and simulated at 300 and 400 K temperatures. In total, we created six systems ($AbMurA_{H2O}$, $AbMurA_{3.5}$ and $AbMurA_{8.0}$ at 300 and 400 K) and generated trajectories at 100 ns. The results were analysed in terms of RMSD,

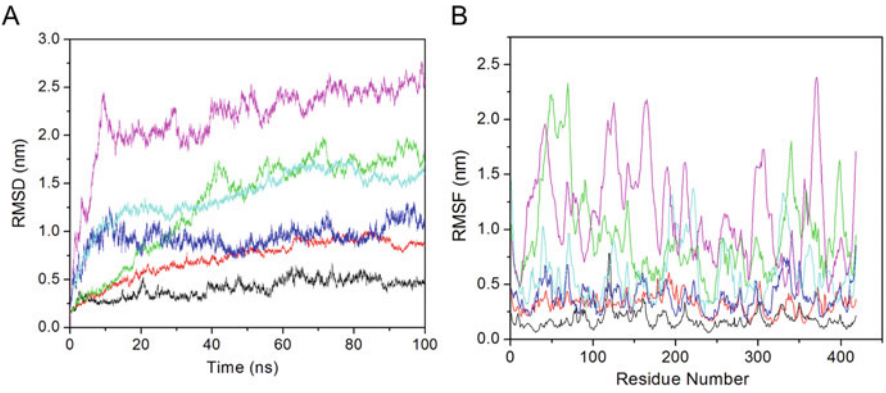

Fig. 2 (**a**) RMSD, (**b**) RMSF. The black, blue, red, green, cyan and magenta represent $AbMurA_{H2O}$ (300 K), $AbMurA_{H2O}$ (400 K), $AbMurA_{3.5}$ (300 K), $AbMurA_{3.5}$ (400 K), $AbMurA_{8.0}$ (300 K) and $AbMurA_{8.0}$ (400 K), respectively

RMSF, Rg, SASA, PCA, structural analysis, and secondary structure analysis. We briefly discuss the results; for a detailed analysis, readers can refer to the original article [69].

We first calculated the RMSD to study the detailed dynamics of the system. At 300 K, the average RMSD value for the $AbMurA_{H2O}$, $AbMurA_{3.5}$ and $AbMurA_{8.0}$ at 300 K were 0.41, 0.71, and 1.30 nm, respectively (Fig. 2a). Figure 2a shows that $AbMurA_{H2O}$ quickly achieved the equilibration state and showed a stable trajectory till 100 ns. The $AbMurA_{3.5}$ showed an increase in the RMSD value initially, while after 40 ns, it achieved the equilibration state. In the case of $AbMurA_{8.0}$, an abrupt pattern was observed till 65 ns and then attained the equilibration state. The average RMSD values represent that urea addition in the systems induces instability in the AbMurA enzyme. We then calculated the RMSD values of $AbMurA_{H2O}$, $AbMurA_{3.5}$ and $AbMurA_{8.0}$ at 400 K (Fig. 2a). 400 K temperature can immediately unfold the protein and provide information on the proper unfolding pathway in the presence of urea. In 400 K, $AbMurA_{H2O}$ attained the equilibration state after 20 ns, while the other two systems, $AbMurA_{3.5}$ and $AbMurA_{8.0}$, achieved the equilibration state after 40 ns and remained stable till 100 ns. The average RMSD values were 0.93, 1.36, and 2.18 nm for $AbMurA_{H2O}$, $AbMurA_{3.5}$ and $AbMurA_{8.0}$. The RMSD result analysis represents that all the systems got the equilibration state and can be further used. It also showed that at 3.5 M concentration of urea, the AbMurA formed an intermediate state, while at 8.0 M of urea, it was completely unfolded.

The RMSF values for the systems were also calculated at 300 and 400 K (Fig. 2b). At 300 K, the RMSF values for the $AbMurA_{H2O}$ were stable, though a higher peak was observed between 115 and 125 residues (with RMSF value between 0.23 and 0.78 nm). When 3.5 M urea was added to the system, RMSF values of >0.5 nm were observed for all the systems. In the case of $AbMurA_{8.0}$, high RMSF values were observed, indicating that the addition of urea induces changes in the structural conformations followed by protein unfolding. At 400 K, an average

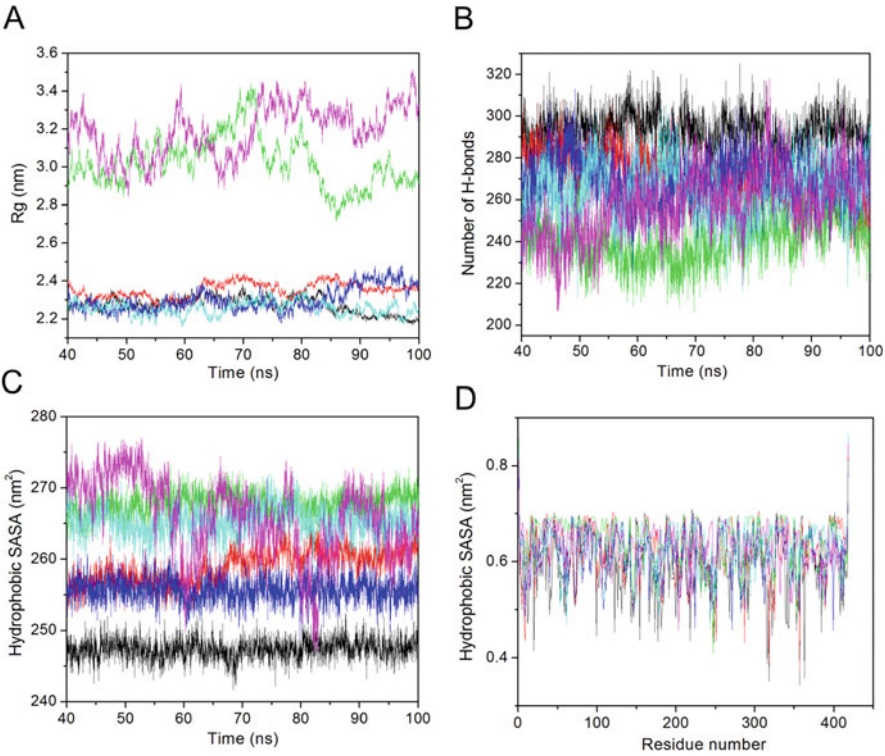

Fig. 3 (**a**) Radius of gyration. (**b**) Number of hydrogen bonds. (**c**) Solvent accessible surface area. (**d**) Solvent accessible surface area versus residues. The black, blue, red, green, cyan and magenta represent $AbMurA_{H2O}$ (300 K), $AbMurA_{H2O}$ (400 K), $AbMurA_{3.5}$ (300 K), $AbMurA_{3.5}$ (400 K), $AbMurA_{8.0}$ (300 K) and $AbMurA_{8.0}$ (400 K), respectively

fluctuation between 0.2 to 0.5 nm was observed for $AbMurA_{H2O}$. High RMSF values of >0.5 nm were observed for residues 35–49, 66–70, 323–352 and 411–148. $AbMurA_{3.5}$ showed RMSF values between 0.5 and 1.0 nm for all the systems. $AbMurA_{8.0}$ showed higher RMSF values for all the residues representing complete structure loss at 8.0 M urea. The overall RMSF analysis indicates that the addition of urea disrupts the original conformation of AbMurA.

We also calculated the Rg values for all the systems using the last 60 ns equilibrated trajectories. Compared to other systems, higher Rg values were observed for 8.0 M urea at 300 and 400 K. For other systems, the Rg values for $AbMurA_{3.5}$ were more than $AbMurA_{H2O}$ (Fig. 3a). The number of hydrogen bonds for all the systems was also calculated (Fig. 3b), which was in the order of $AbMurA_{H20} > AbMurA_{3.5} > AbMurA_{8.0}$. This suggests that the addition of urea leads to the loss of hydrogen bonds. The average number of hydrogen bonds was 270, 264, and 258 for $AbMurA_{H20}$, $AbMurA_{3.5}$, and $AbMurA_{8.0}$, respectively, at 400 K. The SASA values were also analysed (Fig. 3c), which closely agreed with the Rg data. Higher SASA values were observed for the $AbMurA_{3.5}$ and $AbMurA_{8.0}$

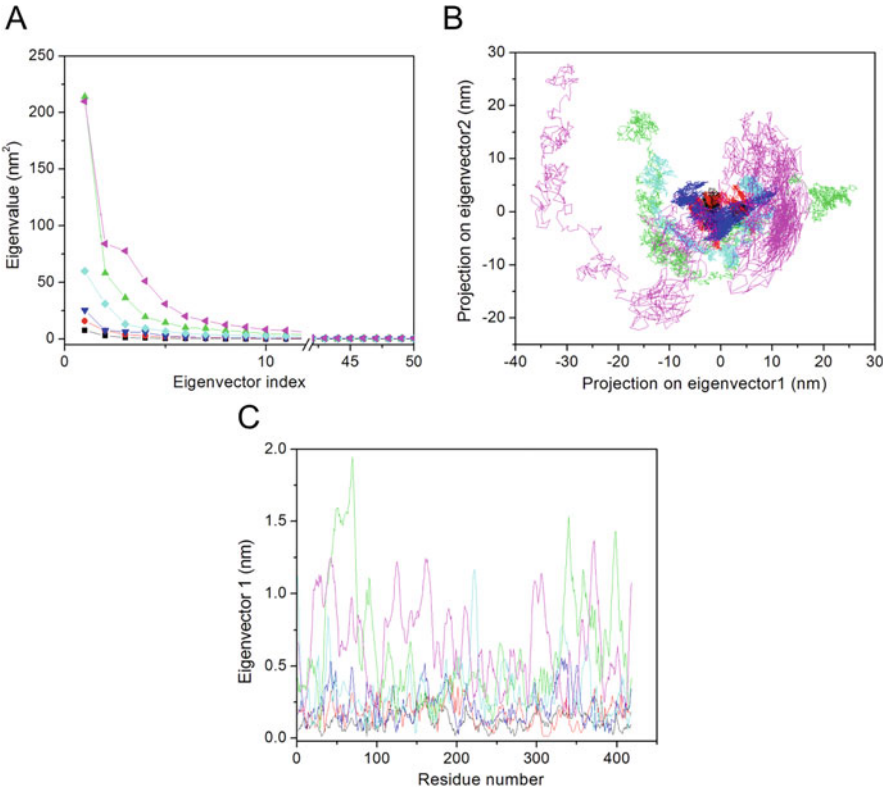

Fig. 4 (**a**) Eigenvalue versus eigenvector. (**b**) 2D project plot. (**c**) eigRMSF values. The black, blue, red, green, cyan and magenta represent $AbMurA_{H2O}$ (300 K), $AbMurA_{H2O}$ (400 K), $AbMurA_{3.5}$ (300 K), $AbMurA_{3.5}$ (400 K), $AbMurA_{8.0}$ (300 K) and $AbMurA_{8.0}$ (400 K), respectively

than $AbMurA_{H20}$, representing the unfolding of the protein. For residual SASA, we analysed the SASA value of tryptophan residue, which indicates that the addition of urea increases the exposure of tryptophan towards the solvent followed by unfolding (Fig. 3d). Collectively, all results suggest that the addition of the urea induces the unfolding of the AbMurA protein.

The PCA was carried out to analyse the correlated motions induced by the addition of urea (Fig. 4). Since the first few eigenvectors represent the overall dynamics of the system, hence first five eigenvectors were considered (Fig. 4a). $AbMurA_{H20}$ showed less correlated motions, while $AbMurA_{3.5}$ and $AbMurA_{8.0}$ showed higher correlated motions. The pattern was the same for both 300 and 400 K temperatures. PCA data also showed a partial unfolding of the protein at 3.5 M urea and complete unfolding at 8.0 M urea. The first two eigenvectors were then taken and plotted (Fig. 4b). The data showed a stable cluster for the $AbMurA_{H20}$ and dispersed clusters for $AbMurA_{3.5}$ and $AbMurA_{8.0}$. Lastly, the eigRMSF values (Fig. 4c) were analysed, which showed a similar pattern to the RMSF values. Higher

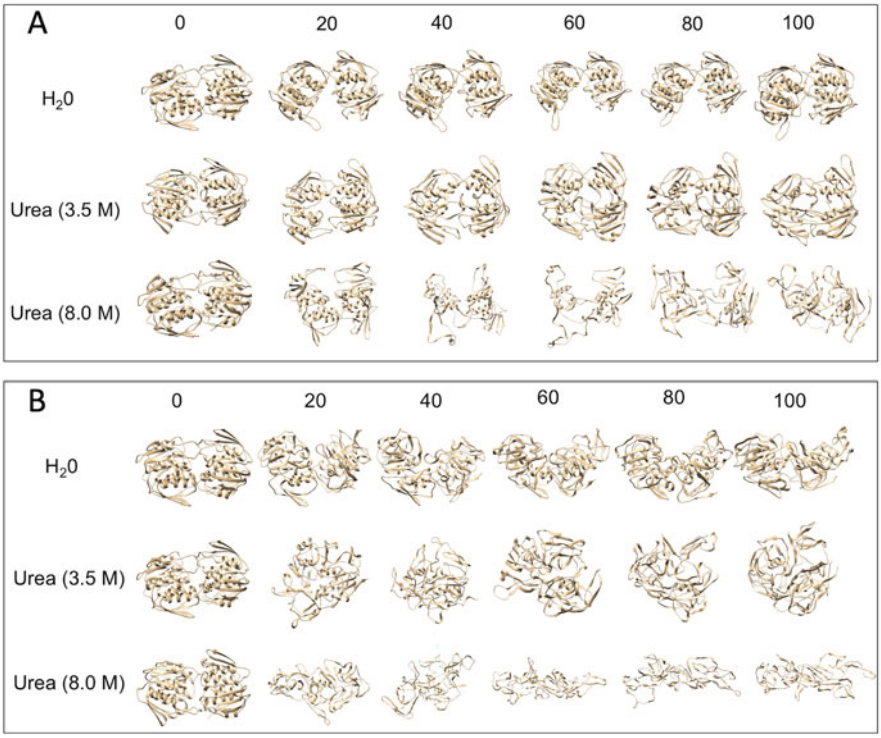

Fig. 5 Time-dependent secondary structural changes. Structural features obtained from the snapshots generated at 20 ns time intervals at (**a**) 300 K and (**b**) 400 K for AbMurA

residue fluctuations were observed in $AbMurA_{3.5}$ and $AbMurA_{8.0}$ systems, while lower fluctuations were observed for $AbMurA_{H20}$. The overall PCA results concluded that at 3.5 M of urea, the AbMurA formed an intermediate folding state, while complete unfolding was observed at 8.0 M urea.

The MD simulation can produce trajectories that can be visually analysed using any visualization software. We analysed the trajectories at 20 ns intervals to obtain a visual representation of the urea-induced unfolding at 300 and 400 K temperatures (Fig. 5). Firstly, we analysed the structural snapshots at 300 K for $AbMurA_{H2O}$, $AbMurA_{3.5}$ and $AbMurA_{8.0}$. It is evident from Fig. 5a that $AbMurA_{H2O}$ did not unfold till 100 ns while there were minor structural changes in the $AbMurA_{3.5}$ intermediate state. The $AbMurA_{8.0}$ started unfolding after 40 ns. It showed the disappearance of the stable secondary structures, such as alpha helices and beta sheets, and an increase in turns and loops. The data showed that 8.0 M urea induces the structural unfolding in the protein. We then analysed the structural changes at 400 K for $AbMurA_{H2O}$, $AbMurA_{3.5}$ and $AbMurA_{8.0}$. The structural snapshots at 20 ns time intervals are shown in Fig. 5b. The data shows that the presence of urea at 400 K temperature induces large structural changes in the protein. At 400 K, the intermediate state at 3.5 M urea also showed structural disruption, while major

changes were observed in the presence of 8.0 M urea. $AbMurA_{8.0}$ showed total disruption of the structure after 40 ns. The data showed the presence of an intermediate state at 3.5 M urea while a complete structure disruption at 8.0 M urea.

The secondary structure analysis was carried out to analyse the secondary structure level changes with respect to time (Fig. 6). The coils, turns and bends were found to be increased at higher concentrations of urea while beta sheets and alpha helices disappeared. First, the secondary structural changes at 300 K were analysed (Fig. 6a). The AbMurA in water showed a stable secondary structure and no major changes throughout the simulation, while at 3.5 M urea, the AbMurA showed a few changes, such as an increase in coils, bends and turns but no major losses in the stable secondary structures. The AbMurA at 8.0 M urea showed much higher turns, coils and bends and loss of helices and sheets. From residues 1–130, we observed the loss of rigid structures and increased bends, turns and coils. The overall analysis showed that at 3.5 M of urea, AbMurA showed minor changes in the secondary structures, while at 8.0 M of urea, major structural changes occurred. The secondary structural changes were also analysed at 400 K for $AbMurA_{H2O}$, $AbMurA_{3.5}$ and $AbMurA_{8.0}$ (Fig. 6b). Here also, it was observed that $AbMurA_{H2O}$ showed stable structures with a few temperature-induced changes. The $AbMurA_{3.5}$ showed an increase in the coils, bends and turns and minor changes in helices and sheets. The $AbMurA_{8.0}$ system showed a much higher number of bends, turns and coils and the disappearance of sheets and helices. Only a few beta sheets were observed, while the alpha helices completely disappeared. The data indicated that in 8.0 M urea, the AbMurA completely lost secondary structures.

The combined spectroscopic and MD simulation data showed the structural characteristics of AbMurA in native ($AbMurA_{H2O}$), intermediate ($AbMurA_{3.5}$) and unfolded ($AbMurA_{8.0}$) states [69]. The data obtained from the MD simulation revealed the atomistic and structural basis of the unfolding of AbMurA, which was not possible using only spectroscopic methods.

6.2 GdnHCl-Induced Unfolding

GdnHCl is another chaotropic agent widely used for denaturation studies of proteins. It can also be added to the MD simulation box, and the structural changes can be captured at different time scales. We discuss a case study from the work of Syed et al. [74]. Firstly, they carried out the unfolding analysis using the series of in vitro experiments and then, for analysing the atomic level structural changes, they carried out the detailed MD simulation analysis. The authors described the folding pattern of the 196–443 residues of human integrin linked kinase (ILK) with 100 ns MD simulation in water, 2.0, 4.0, 6.0, and 8.0 M GdnHCl concentrations. We will discuss key findings from this study related to the MD simulation. They created a total of five MD systems and analysed parameters such as RMSD, RMSF, Rg, SASA, the number of hydrogen bonds, etc.

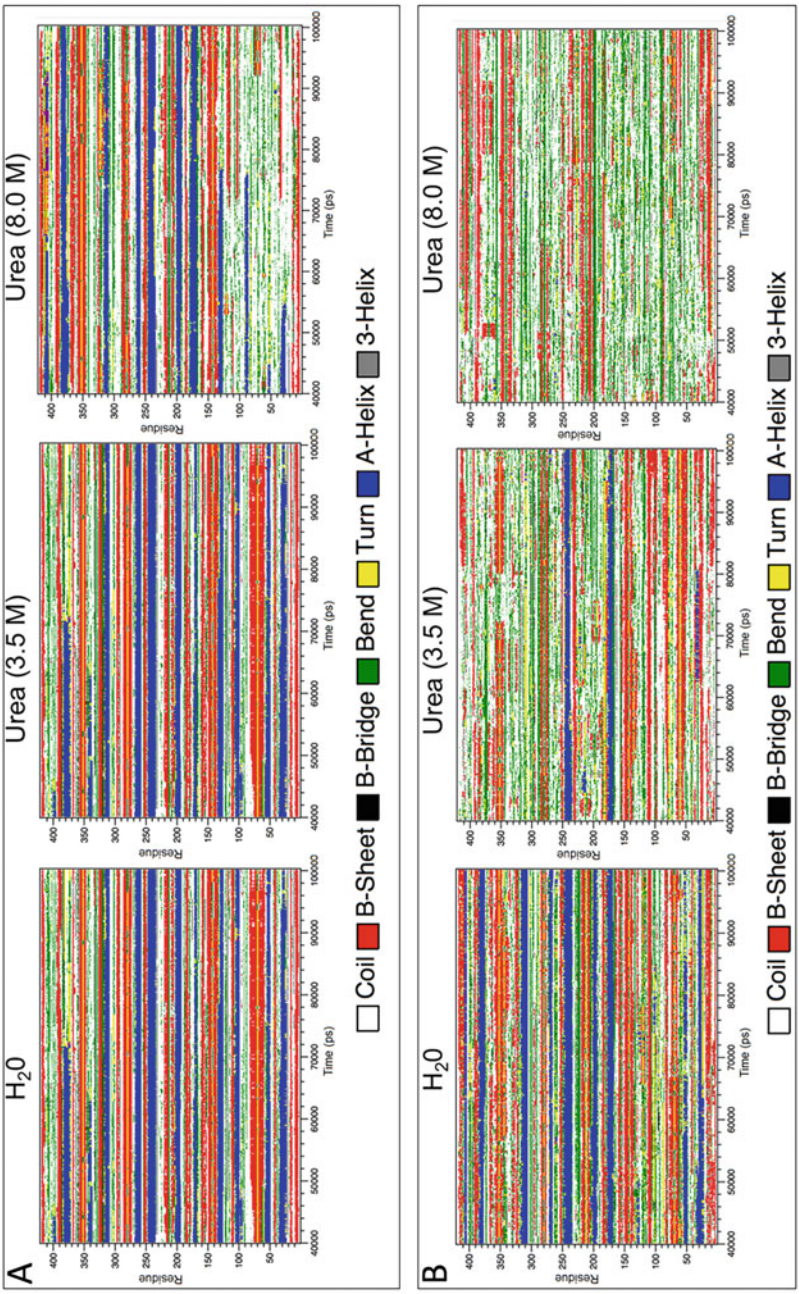

Fig. 6 Evolution of secondary structures of AbMurA at (**a**) 300 K and (**b**) 400 K

Firstly, they calculated the potential energy of the system, where they found that ILK_{H2O}, $ILK_{2.0}$, $ILK_{4.0}$, $ILK_{6.0}$ and $ILK_{8.0}$ showed −2.92196, −358,821, −411,597, −439,100, −1,044,520 kJ/mol energy, respectively. The potential energy of the systems represented that ILK_{H2O} is more stable than GdnHCl systems.

To find the deviation from the initial structure, the authors calculated the RMSD value for all the systems. The average RMSD for ILK_{H2O}, $ILK_{2.0}$, $ILK_{4.0}$, $ILK_{6.0}$ and $ILK_{8.0}$ were 0.33, 0.40, 0.34, 0.27 and 0.36 nm, respectively (Fig. 7a). The figure indicated that the $ILK_{2.0}$, $ILK_{4.0}$ and $ILK_{8.0}$ showed more deviation than ILK_{H2O}. The authors observed less RMSD value for $ILK_{6.0}$. They observed higher changes at 2.0 M GdnHCl concentration throughout the simulation. The $ILK_{4.0}$ and $ILK_{8.0}$ systems showed a little higher RMSD value than ILK in water, representing that at this GdnHCl concentration, partial conformational changes are occurring in the ILK protein. The RMSD analysis showed that all the systems were stable and generated trajectories that can be further utilized for other studies.

After RMSD analysis, the authors calculated the Rg and analysed it in detail. Rg is an important parameter to describe the unfolding pattern of a protein. The average Rg values for the ILK_{H2O}, $ILK_{2.0}$, $ILK_{4.0}$, $ILK_{6.0}$ and $ILK_{8.0}$ were 1.72, 1.72, 1.71, 1.76 and 1.76 nm, respectively. The Rg values were plotted with respect to the time (Fig. 7b) that showed that ILK is getting unfolded at 6.0 and 8.0 M concentrations of GdnHCl while conformation changes occur in the ILK at 4.0 M. The $ILK_{2.0}$ showed a similar Rg value as ILK in water. It indicates that $ILK_{6.0}$ and $ILK_{8.0}$ lost compactness and got unfolded.

To determine the GdnHCl-induced residue level changes, RMSF analysis was performed (Fig. 7c). It was seen that the addition of GdnHCl to the systems alters the original conformation of the protein and induces structural changes. Higher residual changes occurred between residues 221–230, 257–263, and 280–293, including the N- and C-terminals. It represents that GdnHCl disrupts the charge–charge interactions in the protein and induces global changes that lead to the unfolding of the ILK.

The SASA analysis was carried out to analyse the solvent accessible surface area changes induced by the GdnHCl. The average SASA values for ILK_{H2O}, $ILK_{2.0}$, $ILK_{4.0}$, $ILK_{6.0}$ and $ILK_{8.0}$ were 132.31, 132.51, 131.40, 133.04 and 134.09 nm^2, respectively (Fig. 7d). It was observed that $ILK_{6.0}$ and $ILK_{8.0}$ showed higher SASA values, indicating the unfolding of ILK. The $ILK_{2.0}$ and $ILK_{4.0}$ systems showed similar SASA values as the ILK in water. From the overall SASA analysis, it was observed that 6.0 and 8.0 M GdnHCl induces the unfolding in the ILK protein.

The folding of the protein strongly depends on the formation of hydrogen bonds. More number of hydrogen bonds in a protein represents a compact and well-folded structure, while a lesser number of hydrogen bonds represents a less compact and elongated structure. The authors plotted the number of hydrogen bonds with respect to time (Fig. 8). The average number of hydrogen bonds between ILK and water molecules were 420, 389, 346, 328 and 361 for ILK_{H2O}, $ILK_{2.0}$, $ILK_{4.0}$, $ILK_{6.0}$ and $ILK_{8.0}$, respectively (Fig. 8a). The hydrogen bonds between ILK and GdnHCl were also calculated (Fig. 8b). The average number of hydrogen bonds between ILK and GdnHCl was 18, 26, 41 and 30, respectively, for ILK_{H2O}, $ILK_{2.0}$, $ILK_{4.0}$, $ILK_{6.0}$ and $ILK_{8.0}$, respectively. The result indicates that adding GdnHCl decreases the ILK

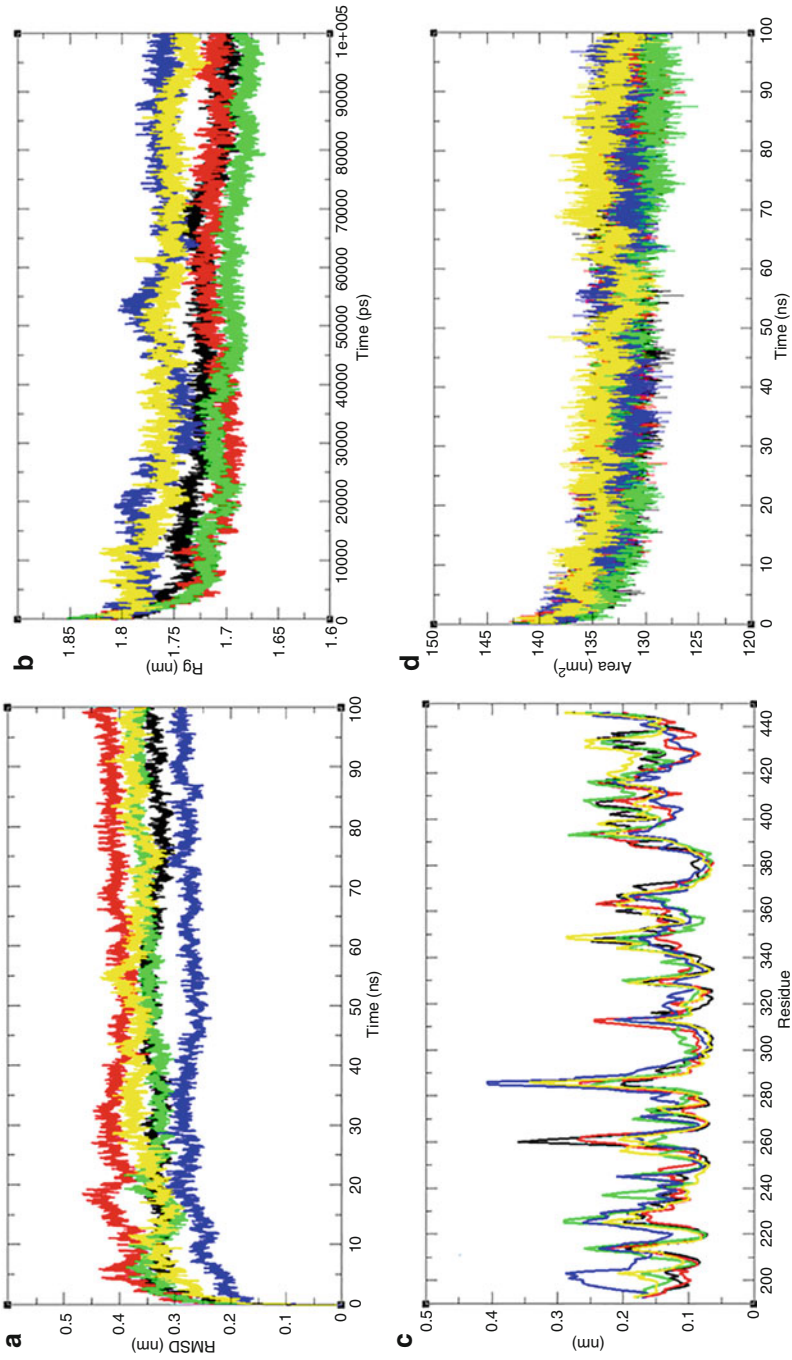

Fig. 7 (**a**) RMSD, (**b**) radius of gyration, (**c**) RMSF, and (**d**) SASA. The ILK_{H2O}, $ILK_{2.0}$, $ILK_{4.0}$, $ILK_{6.0}$ and $ILK_{8.0\ are}$ represented by black, red, green, blue and yellow colours

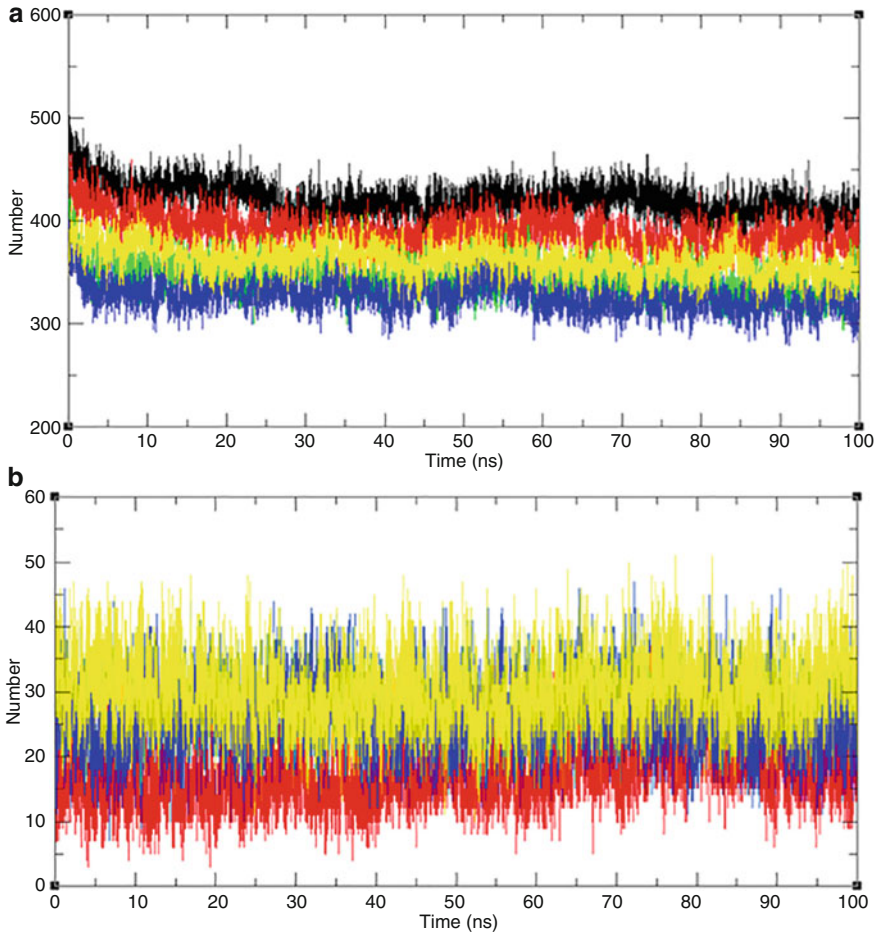

Fig. 8 Number of hydrogen bonds. (**a**) Intramolecular hydrogen bonds of ILK. (**b**) Hydrogen bonds between ILK and GdnHCl. The ILK_{H2O}, $ILK_{2.0}$, $ILK_{4.0}$, $ILK_{6.0}$ and $ILK_{8.0}$ are represented by black, red, green, blue and yellow colours

interaction with water while increasing the interaction with GdnHCl itself. A proper hydration state is required for the solubility of the protein; therefore, it represents that the addition of GdnHCl is disrupting the original conformation of the ILK and inducing the folding in the protein.

From the overall result, the authors concluded that ILK showed higher unfolding at 6.0 and 8.0 M GdnHCl concentrations, representing that the addition of chaotropic agents leads to the unfolding of ILK.

7 Conclusions

Chaotropic agents belong to several chemical families and can induce the denaturation of biomolecules. They follow different mechanisms to alter the structures and denature proteins. Several in vitro spectroscopic methods are available to analyse the effect of the chaotropic agents on proteins, but they cannot provide information on the atomic level changes in the protein structure with respect to time. MD simulation is emerging as an essential tool to track the structural changes and generate thousands of the conformations of a protein. It can also be used to visualize trajectories to analyse the detailed structural level changes. We discussed two case studies using urea and GdnHCl in MD simulation to study the unfolding of proteins in detail. The data showed that the MD simulation result agreed well with the spectroscopic findings and provided several additional atomistic information. Further improvements in the force field and algorithms may help gather precise conformational changes induced by chaotropic agents against the biological macromolecules.

References

1. A. Fershi, *Structure and Mechanism in Protein Science: A Guide to Enzyme Catalysis and Protein Folding* (W.H. Freeman, New York, 1999)
2. W. Kauzmann, Some factors in the interpretation of protein denaturation. Adv. Protein Chem. **14**, 1–63 (1959). https://doi.org/10.1016/S0065-3233(08)60608-7
3. H.S. Frank, F. Franks, Structural approach to the solvent power of water for hydrocarbons; urea as a structure breaker. J. Chem. Phys. **48**, 4746–4757 (1968). https://doi.org/10.1063/1.1668057
4. D.O.V. Alonso, K.A. Dill, Solvent denaturation and stabilization of globular proteins. Biochemistry **30**, 5974–5985 (1991). https://doi.org/10.1021/bi00238a023
5. A. Caflisch, M. Karplus, Molecular dynamics simulation of protein denaturation: solvation of the hydrophobic cores and secondary structure of barnase. Proc. Natl. Acad. Sci. U S A **91**, 1746–1750 (1994). https://doi.org/10.1073/pnas.91.5.1746
6. A. Wallqvist, D.G. Covell, D. Thirumalai, Hydrophobic interactions in aqueous urea solutions with implications for the mechanism of protein denaturation. J. Am. Chem. Soc. **120**, 427–428 (1998). https://doi.org/10.1021/ja972053v
7. R. Chitra, P.E. Smith, Preferential interactions of cosolvents with hydrophobic solutes. J. Phys. Chem. B **105**, 11513–11522 (2001). https://doi.org/10.1021/jp012354y
8. S. Shimizu, H.S. Chan, Origins of protein denatured state compactness and hydrophobic clustering in aqueous urea: inferences from nonpolar potentials of mean force. Proteins **49**, 560–566 (2002). https://doi.org/10.1002/prot.10263
9. B.J. Bennion, V. Daggett, The molecular basis for the chemical denaturation of proteins by urea. Proc. Natl. Acad. Sci. U S A **100**, 5142–5147 (2003). https://doi.org/10.1073/pnas.0930122100
10. S. Kunugi, N. Tanaka, Cold denaturation of proteins under high pressure. Biochim. Biophys. Acta **1595**, 329–344 (2002). https://doi.org/10.1016/s0167-4838(01)00354-5
11. M.I. Marqués, J.M. Borreguero, H.E. Stanley, N.V. Dokholyan, Possible mechanism for cold denaturation of proteins at high pressure. Phys. Rev. Lett. **91**, 138103 (2003). https://doi.org/10.1103/PhysRevLett.91.138103
12. J.S. Yang, W.W. Chen, J. Skolnick, E.I. Shakhnovich, All-atom ab initio folding of a diverse set of proteins. Structure **1993**(15), 53–63 (2007). https://doi.org/10.1016/j.str.2006.11.010

13. K.A. Dill, S.B. Ozkan, M.S. Shell, T.R. Weikl, The protein folding problem. Annu. Rev. Biophys. **37**, 289–316 (2008). https://doi.org/10.1146/annurev.biophys.37.092707.153558
14. V. Daggett, A. Fersht, The present view of the mechanism of protein folding. Nat. Rev. Mol. Cell Biol. **4**, 497–502 (2003). https://doi.org/10.1038/nrm1126
15. K. Prince, S. Sasidharan, N. Nag, T. Tripathi, P. Saudagar, Integration of spectroscopic and computational data to analyze protein structure, function, folding, and dynamics, in *Advanced Spectroscopic Methods to Study Biomolecular Structure and Dynamics*, ed. by P. Saudagar, T. Tripathi, (Academic Press, San Diego, 2023), pp. 483–502. https://doi.org/10.1016/B978-0-323-99127-8.00018-0
16. P.L. Freddolino, A.S. Arkhipov, S.B. Larson, A. McPherson, K. Schulten, Molecular dynamics simulations of the complete satellite tobacco mosaic virus. Structure **14**, 437–449 (2006). https://doi.org/10.1016/j.str.2005.11.014
17. M. Levitt, R. Sharon, Accurate simulation of protein dynamics in solution. Proc. Natl. Acad. Sci. **85**, 7557–7561 (1988). https://doi.org/10.1073/pnas.85.20.7557
18. D.A.C. Beck, D.O.V. Alonso, V. Daggett, A microscopic view of peptide and protein solvation. Biophys. Chem. **100**, 221–237 (2003). https://doi.org/10.1016/s0301-4622(02)00283-1
19. V. Daggett, Protein folding−simulation. Chem. Rev. **106**, 1898–1916 (2006). https://doi.org/10.1021/cr0404242
20. C.B. Anfinsen, Principles that govern the folding of protein chains. Science **181**, 223–230 (1973). https://doi.org/10.1126/science.181.4096.223
21. T. Tripathi, Calculation of thermodynamic parameters of protein unfolding using far-ultraviolet circular dichroism. J. Protein. Proteomics **4**(2), 85–91 (2013)
22. B. Honig, Protein folding: from the levinthal paradox to structure prediction. J. Mol. Biol. **293**, 283–293 (1999). https://doi.org/10.1006/jmbi.1999.3006
23. D.B. Singh, T. Tripathi (eds.), *Frontiers in Protein Structure, Function, and Dynamics* (Springer, Singapore, 2020). https://doi.org/10.1007/978-981-15-5530-5
24. B. Berger, T. Leighton, Protein folding in the hydrophobic-hydrophilic (HP) model is NP-complete. J. Comput. Biol. **5**, 27–40 (1998). https://doi.org/10.1089/cmb.1998.5.27
25. So much more to know. Science **309**, 78–102 (2005). https://doi.org/10.1126/science.309.5731.78b
26. J.D. Bryngelson, J.N. Onuchic, N.D. Socci, P.G. Wolynes, Funnels, pathways, and the energy landscape of protein folding: a synthesis. Proteins **21**, 167–195 (1995). https://doi.org/10.1002/prot.340210302
27. K.A. Dill, H.S. Chan, From Levinthal to pathways to funnels. Nat. Struct. Biol. **4**, 10–19 (1997). https://doi.org/10.1038/nsb0197-10
28. J. Schonbrun, K.A. Dill, Fast protein folding kinetics. Proc. Natl. Acad. Sci. U S A **100**, 12678–12682 (2003). https://doi.org/10.1073/pnas.1735417100
29. H. Kaya, H.S. Chan, Explicit-chain model of native-state hydrogen exchange: Implications for event ordering and cooperativity in protein folding. Proteins **58**, 31–44 (2005). https://doi.org/10.1002/prot.20286
30. P. Bhaganna, R.J.M. Volkers, A.N.W. Bell, K. Kluge, D.J. Timson, J.W. McGrath, H.J. Ruijssenaars, J.E. Hallsworth, Hydrophobic substances induce water stress in microbial cells. Microb. Biotechnol. **3**, 701–716 (2010). https://doi.org/10.1111/j.1751-7915.2010.00203.x
31. K.D. Collins, Charge density-dependent strength of hydration and biological structure. Biophys. J. **72**, 65–76 (1997)
32. G. Salvi, P. De Los Rios, M. Vendruscolo, Effective interactions between chaotropic agents and proteins. Proteins **61**, 492–499 (2005). https://doi.org/10.1002/prot.20626
33. J.A. McCammon, B.R. Gelin, M. Karplus, Dynamics of folded proteins. Nature **267**, 585–590 (1977). https://doi.org/10.1038/267585a0
34. A. Warshel, M. Levitt, Theoretical studies of enzymic reactions: dielectric, electrostatic and steric stabilization of the carbonium ion in the reaction of lysozyme. J. Mol. Biol. **103**, 227–249 (1976). https://doi.org/10.1016/0022-2836(76)90311-9

35. D. Roccatano, A. Barthel, M. Zacharias, Structural flexibility of the nucleosome core particle at atomic resolution studied by molecular dynamics simulation. Biopolymers **85**, 407–421 (2007). https://doi.org/10.1002/bip.20690
36. S. Sharma, F. Ding, N.V. Dokholyan, Multiscale modeling of nucleosome dynamics. Biophys. J. **92**, 1457–1470 (2007). https://doi.org/10.1529/biophysj.106.094805
37. I. Tinoco, J.-D. Wen, Simulation and analysis of single-ribosome translation. Phys. Biol. **6**, 025006 (2009). https://doi.org/10.1088/1478-3975/6/2/025006
38. R. Brandman, Y. Brandman, V.S. Pande, A-site residues move independently from P-site residues in all-atom molecular dynamics simulations of the 70S bacterial ribosome. PLoS One **7**, e29377 (2012). https://doi.org/10.1371/journal.pone.0029377
39. T. Tripathi, V.K. Dubey, *Advances in Protein Molecular and Structural Biology Methods* (Academic Press, London, 2022)
40. M. Orozco, L. Orellana, A. Hospital, A.N. Naganathan, A. Emperador, O. Carrillo, J.L. Gelpí, Coarse-grained representation of protein flexibility. Foundations, successes, and shortcomings. Adv. Protein Chem. Struct. Biol. **85**, 183–215 (2011). https://doi.org/10.1016/B978-0-12-386485-7.00005-3
41. T. Lazaridis, M. Karplus, Effective energy function for proteins in solution. Proteins **35**, 133–152 (1999). https://doi.org/10.1002/(sici)1097-0134(19990501)35:2<133::aid-prot1>3.0.co;2-n
42. B. Roux, T. Simonson, Implicit solvent models. Biophys. Chem. **78**, 1–20 (1999). https://doi.org/10.1016/s0301-4622(98)00226-9
43. U. Haberthür, A. Caflisch, FACTS: fast analytical continuum treatment of solvation. J. Comput. Chem. **29**, 701–715 (2008). https://doi.org/10.1002/jcc.20832
44. M. Orozco, F.J. Luque, Theoretical methods for the description of the solvent effect in biomolecular systems. Chem. Rev. **100**, 4187–4226 (2000). https://doi.org/10.1021/cr990052a
45. T. Luchko, S. Gusarov, D.R. Roe, C. Simmerling, D.A. Case, J. Tuszynski, A. Kovalenko, Three-dimensional molecular theory of solvation coupled with molecular dynamics in Amber. J. Chem. Theory Comput. **6**, 607–624 (2010). https://doi.org/10.1021/ct900460m
46. R. Anandakrishnan, A. Drozdetski, R.C. Walker, A.V. Onufriev, Speed of conformational change: comparing explicit and implicit solvent molecular dynamics simulations. Biophys. J. **108**, 1153–1164 (2015). https://doi.org/10.1016/j.bpj.2014.12.047
47. J. Hermans, H.J.C. Berendsen, W.F. Van Gunsteren, J.P.M. Postma, A consistent empirical potential for water–protein interactions. Biopolymers **23**, 1513–1518 (1984). https://doi.org/10.1002/bip.360230807
48. A.D. MacKerell Jr., J. Wiorkiewicz-Kuczera, M. Karplus, An all-atom empirical energy function for the simulation of nucleic acids. J. Am. Chem. Soc. **117**, 11946–11975 (1995). https://doi.org/10.1021/ja00153a017
49. K.-H. Ott, B. Meyer, Parametrization of GROMOS force field for oligosaccharides and assessment of efficiency of molecular dynamics simulations. J. Comput. Chem. **17**, 1068–1084 (1996). https://doi.org/10.1002/(SICI)1096-987X(199606)17:8<1068::AID-JCC14>3.0.CO;2-A
50. A.D. MacKerell, D. Bashford, M. Bellott, R.L. Dunbrack, J.D. Evanseck, M.J. Field, S. Fischer, J. Gao, H. Guo, S. Ha, D. Joseph-McCarthy, L. Kuchnir, K. Kuczera, F.T. Lau, C. Mattos, S. Michnick, T. Ngo, D.T. Nguyen, B. Prodhom, W.E. Reiher, B. Roux, M. Schlenkrich, J.C. Smith, R. Stote, J. Straub, M. Watanabe, J. Wiórkiewicz-Kuczera, D. Yin, M. Karplus, All-atom empirical potential for molecular modeling and dynamics studies of proteins. J. Phys. Chem. B **102**, 3586–3616 (1998). https://doi.org/10.1021/jp973084f
51. W.D. Cornell, P. Cieplak, C.I. Bayly, I.R. Gould, K.M. Merz, D.M. Ferguson, D.C. Spellmeyer, T. Fox, J.W. Caldwell, P.A. Kollman, A second generation force field for the simulation of proteins, nucleic acids, and organic molecules. J. Am. Chem. Soc. **117**, 5179–5197 (1995). https://doi.org/10.1021/ja00124a002
52. G.A. Kaminski, R.A. Friesner, J. Tirado-Rives, W.L. Jorgensen, Evaluation and reparametrization of the OPLS-AA force field for proteins via comparison with accurate

quantum chemical calculations on peptides. J. Phys. Chem. B **105**, 6474–6487 (2001). https://doi.org/10.1021/jp003919d
53. M. Rueda, C. Ferrer-Costa, T. Meyer, A. Pérez, J. Camps, A. Hospital, J.L. Gelpí, M. Orozco, A consensus view of protein dynamics. Proc. Natl. Acad. Sci. U S A **104**, 796–801 (2007). https://doi.org/10.1073/pnas.0605534104
54. A. Perez, F. Lankas, F.J. Luque, M. Orozco, Towards a molecular dynamics consensus view of B-DNA flexibility. Nucleic Acids Res. **36**, 2379–2394 (2008). https://doi.org/10.1093/nar/gkn082
55. B.R. Brooks, C.L. Brooks, A.D. Mackerell, L. Nilsson, R.J. Petrella, B. Roux, Y. Won, G. Archontis, C. Bartels, S. Boresch, A. Caflisch, L. Caves, Q. Cui, A.R. Dinner, M. Feig, S. Fischer, J. Gao, M. Hodoscek, W. Im, K. Kuczera, T. Lazaridis, J. Ma, V. Ovchinnikov, E. Paci, R.W. Pastor, C.B. Post, J.Z. Pu, M. Schaefer, B. Tidor, R.M. Venable, H.L. Woodcock, X. Wu, W. Yang, D.M. York, M. Karplus, CHARMM: the biomolecular simulation program. J. Comput. Chem. **30**, 1545–1614 (2009). https://doi.org/10.1002/jcc.21287
56. M.J. Abraham, T. Murtola, R. Schulz, S. Páll, J.C. Smith, B. Hess, E. Lindahl, GROMACS: High performance molecular simulations through multi-level parallelism from laptops to supercomputers. SoftwareX **1–2**, 19–25 (2015). https://doi.org/10.1016/j.softx.2015.06.001
57. D.A. Case, T.E. Cheatham, T. Darden, H. Gohlke, R. Luo, K.M. Merz, A. Onufriev, C. Simmerling, B. Wang, R.J. Woods, The Amber biomolecular simulation programs. J. Comput. Chem. **26**, 1668–1688 (2005). https://doi.org/10.1002/jcc.20290
58. M.T. Nelson, W. Humphrey, A. Gursoy, A. Dalke, L.V. Kalé, R.D. Skeel, K. Schulten, NAMD: a parallel, object-oriented molecular dynamics program. Int. J. Supercomput. Appl. High Perform. Comput. **10**, 251–268 (1996). https://doi.org/10.1177/109434209601000401
59. P. Larsson, B. Hess, E. Lindahl, Algorithm improvements for molecular dynamics simulations. WIREs Comput. Mol. Sci. **1**, 93–108 (2011). https://doi.org/10.1002/wcms.3
60. M.J. Harvey, G. Giupponi, G.D. Fabritiis, ACEMD: accelerating biomolecular dynamics in the microsecond time scale. J. Chem. Theory Comput. **5**, 1632–1639 (2009). https://doi.org/10.1021/ct9000685
61. H. Shukla, R. Shukla, A. Sonkar, T. Pandey, T. Tripathi, Distant Phe345 mutation compromises the stability and activity of mycobacterium tuberculosis isocitrate lyase by modulating its structural flexibility. Sci. Rep. **7**, 1058 (2017). https://doi.org/10.1038/s41598-017-01235-z
62. H. Shukla, R. Shukla, A. Sonkar, T. Tripathi, Alterations in conformational topology and interaction dynamics caused by L418A mutation leads to activity loss of mycobacterium tuberculosis isocitrate lyase. Biochem. Biophys. Res. Commun. **490**, 276–282 (2017). https://doi.org/10.1016/j.bbrc.2017.06.036
63. R. Shukla, H. Shukla, T. Tripathi, Activity loss by H46A mutation in mycobacterium tuberculosis isocitrate lyase is due to decrease in structural plasticity and collective motions of the active site. Tuberculosis **108**, 143–150 (2018). https://doi.org/10.1016/j.tube.2017.11.013
64. R. Shukla, T.R. Singh, Virtual screening, pharmacokinetics, molecular dynamics and binding free energy analysis for small natural molecules against cyclin-dependent kinase 5 for Alzheimer's disease. J. Biomol. Struct. Dyn. **38**, 248–262 (2020). https://doi.org/10.1080/07391102.2019.1571947
65. R. Shukla, T.R. Singh, High-throughput screening of natural compounds and inhibition of a major therapeutic target HsGSK-3β for Alzheimer's disease using computational approaches. J. Genet. Eng. Biotechnol. **19**, 61 (2021). https://doi.org/10.1186/s43141-021-00163-w
66. R. Shukla, P.B. Chetri, A. Sonkar, M.Y. Pakharukova, V.A. Mordvinov, T. Tripathi, Identification of novel natural inhibitors of opisthorchis felineus cytochrome P450 using structure-based screening and molecular dynamic simulation. J. Biomol. Struct. Dyn. **36**, 3541–3556 (2018). https://doi.org/10.1080/07391102.2017.1392897
67. R. Shukla, H. Shukla, T. Tripathi, Structural and energetic understanding of novel natural inhibitors of Mycobacterium tuberculosis malate synthase. J. Cell. Biochem. **120**(2), 2469–2482 (2019). https://doi.org/10.1002/jcb.27538

68. J. Kalita, R. Shukla, T. Tripathi, Structural basis of urea-induced unfolding of Fasciola gigantica glutathione S-transferase. J. Cell. Physiol. **234**, 4491–4503 (2019). https://doi.org/10.1002/jcp.27253
69. A. Sonkar, H. Shukla, R. Shukla, J. Kalita, T. Tripathi, Unfolding of acinetobacter baumannii MurA proceeds through a metastable intermediate: a combined spectroscopic and computational investigation. Int. J. Biol. Macromol. **126**, 941–951 (2019). https://doi.org/10.1016/j.ijbiomac.2018.12.124
70. P.B. Chetri, R. Shukla, J.M. Khan, A.K. Padhi, T. Tripathi, Unraveling the structural basis of urea-induced unfolding of Fasciola gigantica cytosolic malate dehydrogenase. J. Mol. Liq. **349**, 118170 (2022). https://doi.org/10.1016/j.molliq.2021.118170
71. R. Shukla, T. Tripathi, Molecular dynamics simulation in drug discovery: opportunities and challenges, in *Innovations and Implementations of Computer Aided Drug Discovery Strategies in Rational Drug Design*, ed. by S.K. Singh, (Springer, Singapore, 2021), pp. 295–316. https://doi.org/10.1007/978-981-15-8936-2_12
72. R. Shukla, T. Tripathi, Molecular dynamics simulation of protein and protein–ligand complexes, in *Computer-Aided Drug Design—An Overview*, ed. by D.B. Singh, (Springer, Singapore, 2020), pp. 133–161. https://doi.org/10.1007/978-981-15-6815-2_7
73. P. Saudagar, T. Tripathi, *Advanced Spectroscopic Methods to Study Biomolecular Structure and Dynamics* (Academic Press, San Diego, 2023)
74. S.B. Syed, F.I. Khan, S.H. Khan, S. Srivastava, G.M. Hasan, K.A. Lobb, A. Islam, M.I. Hassan, F. Ahmad, Unravelling the unfolding mechanism of human integrin linked kinase by GdmCl-induced denaturation. Int. J. Biol. Macromol. **117**, 1252–1263 (2018). https://doi.org/10.1016/j.ijbiomac.2018.06.025